Inorg. Chem. **2007**, *46*, 2519–2529

Inorganic Chemistry
Article

Novel Linear Transition Metal Clusters of a Heptadentate Bis-β-diketone Ligand

Guillem Aromí,*[†] Patrick Gamez,[‡] J. Krzystek,[§] Huub Kooijman,[||] Anthony L. Spek,[||]
Elizabeth J. MacLean,[⊥] Simon J. Teat,[⊥,#] and Harriott Nowell[▽]

Departament de Química Inorgànica, Universitat de Barcelona, Diagonal 647, 08028 Barcelona, Spain, Leiden Institute of Chemistry, Gorlaeus Laboratories, Leiden University, PO Box 9502, 2300 RA Leiden, The Netherlands, National High Magnetic Field Laboratory, Florida State University, Tallahassee, Florida 32310, Bijvoet Center for Biomolecular Research, Crystal and Structural Chemistry, Utrecht University, Padualaan 8, 3584 CH Utrecht, The Netherlands, CCLRC Daresbury Laboratory, Warrington, Cheshire WA4 4AD, U.K., Advance Light Source, Lawrence Berkeley Lab, 1 Cyclotron Rd, MS2-400, Berkeley, California 94720, and Diamond Light Source, Ltd., Diamond House, Chilton, Didcot, Oxfordshire OX11 0DE, U.K.

Received October 30, 2006

The synthesis and the structure of the new potentially heptadentate ligand 1,3-bis-(3-oxo-3-(2-hydroxyphenyl)-propionyl)-2-methoxybenzene (**H_5L**) is described. The reaction in pyridine or DMF of this ligand with various $M(AcO)_2$ salts ($M = Ni^{II}$, Co^{II}, Mn^{II}) leads to very different products depending on the metal. Thus, the dinuclear complexes $[M_2(H_3L)_2(py)_4]$ ($M = Ni^{II}$, **1**; Co^{II}, **2**) or the linear zigzag tetranuclear clusters $[Mn_4(H_2L)_2(AcO)_2(py)_5]$ (**3**) and $[Mn_4(H_2L)_2(AcO)_2(dmf)_4]$ (**4**) have been synthesized and characterized crystallographically. Slow oxidation of complex **3** leads to the formation of the novel mixed-valence linear complex $[Mn_3(HL)_2(py)_6]$ (**5**), displaying an unprecedented asymmetric $Mn^{III}Mn^{III}Mn^{II}$ topology. The coordination geometry of complexes **1** to **5** has been analyzed and discussed by means of continuous shape measures. Magnetic measurements of **3** and **5** demonstrate that the metals within these complexes weakly interact magnetically with coupling constants of $J_1 = -1.13$ cm^{-1} and $J_2 = -0.43$ cm^{-1} ($S = 0$) for complex **3** and $J_1 = -5.4$ cm^{-1} and $J_2 = -0.4$ cm^{-1} ($S = {}^5/_2$) for complex **5** (using the $H = -\Sigma 2J_{ij}S_iS_j$ convention). These results are consistent with X-band EPR measurements on these compounds.

Introduction

One of the pillars of molecular magnetism is the synthesis of novel materials aimed at discovering new properties or deepening the understanding of known magnetic phenomena. For example, since the discovery of single-molecule magnets (SMMs)[1] or single-chain magnets[2] vast efforts have been made in the synthetic arena to increase the spin state of molecules or control the factors that govern the magnetoanisotropy of these systems.[3,4] Thus, in the past decade the reports on novel discrete and extended coordination compounds with relevance to magnetism have proliferated, boosting the discipline enormously. It is interesting to note that most clusters prepared with this aim are made by self-assembly from paramagnetic metal ions and small bridging ligands, although this approach rarely allows the prediction of the final products structure.[5−9] Some authors, however, have engaged in the design and synthesis of complicated multidentate ligands to use in reactions with transition metals,

---

* To whom correspondence should be addressed. E-mail: guillem.aromi@qi.ub.es.

[†] Universitat de Barcelona.

[‡] Leiden University.

[§] Florida State University.

[||] Utrecht University.

[⊥] Daresbury Laboratory.

[#] Lawrence Berkeley Lab.

[▽] Diamond House.

(1) Sessoli, R.; Tsai, H. L.; Schake, A. R.; Wang, S. Y.; Vincent, J. B.; Folting, K.; Gatteschi, D.; Christou, G.; Hendrickson, D. N. *J. Am. Chem. Soc.* **1993**, *115*, 1804−1816.

(2) Caneschi, A.; Gatteschi, D.; Lalioti, N.; Sangregorio, C.; Sessoli, R.; Venturi, G.; Vindigni, A.; Rettori, A.; Pini, M. G.; Novak, M. A. *Angew. Chem., Int. Ed.* **2001**, *40*, 1760−1763.

(3) Aromí, G.; Brechin, E. K. *Struct. Bonding* **2006**, *122*, 1−67.

(4) Coulon, C.; Misayaka, H.; Clérac, R. *Struct. Bonding* **2006**, *122*, 163−206.

(5) Milios, C. J.; Stamatatos, T. C.; Perlepes, S. P. *Polyhedron* **2006**, *25*, 134−194.

(6) Winpenny, R. E. P. *Adv. Inorg. Chem.* **2001**, *52*, 1.

(7) Winpenny, R. E. P. *J. Chem. Soc., Dalton Trans.* **2002**, 1−10.

(8) Brechin, E. K. *Chem. Commun.* **2005**, 5141−5153.

10.1021/ic062075v CCC: $37.00

Scheme 1

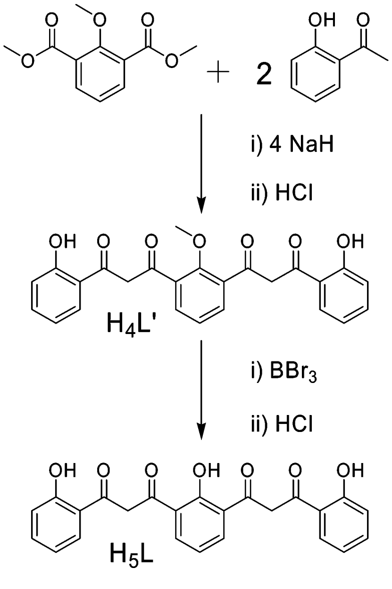

with the aim of enforcing certain topological patterns or even introducing functionality aspects to the resulting coordination complexes.[10−13] For a few years, some of us have devoted efforts to designing and synthesizing a class of ligands displaying linear arrays of oxygen donors, based on the adjacent disposition of phenol and 1,3-diketone groups, with the aim of favoring the formation of chains of closely spaced transition metals.[14,15] This topology is of relevance in molecular magnetism, since it might lead to highly anisotropic systems and allow a better understanding of the phenomenon of magnetic anisotropy. Indeed, one of the postulated strategies to improve the properties of SMMs is to aim at species with increased magnetoanisotropy. In this sense, it is important to understand the factors that enhance it and to reach the ability to control these within synthetic schemes. The first members of the family of poly-1,3-diketone ligands mentioned above exhibited five and six O-donors in a linear fashion. Different degrees of occupancy of their coordination pockets have led to several complexes, which are dinuclear[16] or exhibit chains with three[17] or four members.[18] We report here the synthesis and structure of the longest ligand made of this family, $\mathbf{H_5L}$ (1,3-bis-(3-oxo-3-(2-hydroxyphenyl)-propionyl)-2-methoxybenzene), containing five ionizable protons and a string of seven oxygen donors in the form of two 1,3-diketones and three phenol adjacent groups. The reactivity of $\mathbf{H_5L}$ toward $M(AcO)_2$ (M = Ni^{II}, Co^{II}, Mn^{II}) was found to vary dramatically depending on the metal. Thus, dinuclear complexes were obtained with nickel(II) and cobalt(II) whereas manganese(II) led to a tetranuclear cluster comprising a very interesting $[Mn_4O_6]$ core in the form of a zigzag chain. On the other hand, the mixture Mn^{III}/Mn^{II} favors the formation of a unique mixed-valence linear compound exhibiting a rare asymmetric $[Mn^{III}-Mn^{III}-Mn^{II}]$ sequence. The synthesis and structure of these compounds are described, as well as the magnetic properties of the manganese aggregates. Some of these results have been previously communicated.[19]

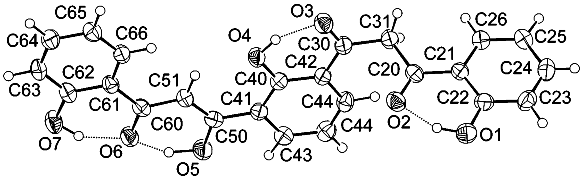

Figure 1. Labeled ORTEP representation of $\mathbf{H_5L}$ at the 50% probability level. Hydrogen bonds are shown as dashed lines.

Results and Discussion

Synthesis. The heptadentate ligand $\mathbf{H_5L}$ (Scheme 1) was prepared from the related bis-β-diketone/methoxy-ether ($\mathbf{H_4L'}$) derivative through ether cleavage by BBr_3. The latter polyketone was synthesized through the coupling between the appropriate diester (dimethyl 2-methoxyisophthalate) and the corresponding ketone (2-hydroxyacetophenone) by means of a Claisen condensation (Scheme 1).[15] In this reaction, the product is obtained as the tetra-anionic sodium salt together with other salts such as NaMeO, and the system is later acidified in order to obtain the neutral form of the sought molecule. Invariably, the target compound was obtained together with approximately 15−20% of the monocoupled derivative. The former could only be isolated pure by solubilization of the impurity in acetone. The conversion to the bis-β-diketone/trisphenol derivative ($\mathbf{H_5L}$) necessitated 1.5 equiv of BBr_3, albeit each mole of the tribromide can potentially cleave 3 mol of ether.[20] Very likely, the formation of the orthoboric ester necessary for the process to occur with maximal efficiency is prevented for steric reasons. Mass spectrometry produced solid evidence for the formation of the desired product. ^{1}H NMR spectroscopy, however, revealed a lower symmetry than that suggested in Scheme 1, presumably as a consequence of the particular keto−enolic

---

(9) Aromí, G.; Aubin, S. M. J.; Bolcar, M. A.; Christou, G.; Eppley, H. J.; Folting, K.; Hendrickson, D. N.; Huffman, J. C.; Squire, R. C.; Tsai, H. L.; Wang, S.; Wemple, M. W. *Polyhedron* **1998**, *17*, 3005−3020.

(10) Yoshino, A.; Miyagi, T.; Asato, E.; Mikuriya, M.; Sakata, Y.; Sugiura, K.; Iwasaki, K.; Hino, S.; Hino, D. *Chem. Commun.* **2000**, 1475−1476.

(11) Thompson, L. K.; Kelly, T. L.; Dawe, L. N.; Grove, H.; Lemaire, M. T.; Howard, J. A. K.; Spencer, E. C.; Matthews, C. J.; Onions, S. T.; Coles, S. J.; Horton, P. N.; Hursthouse, M. B.; Light, M. E. *Inorg. Chem.* **2004**, *43*, 7605−7616.

(12) Peng, S. M.; Wang, C. C.; Jang, Y. L.; Chen, Y. H.; Li, F. Y.; Mou, C. Y.; Leung, M. K. *J. Magn. Magn. Mater.* **2000**, *209*, 80−83.

(13) Ottenwaelder, X.; Cano, J.; Journaux, Y.; Riviere, E.; Brennan, C.; Nierlich, M.; Ruiz-Garcia, R. *Angew. Chem., Int. Ed.* **2004**, *43*, 850−852.

(14) Aromí, G.; Boldron, C.; Gamez, P.; Roubeau, O.; Kooijman, H.; Spek, A. L.; Stoeckli-Evans, H.; Ribas, J.; Reedijk, J. *Dalton Trans.* **2004**, 3586−3592.

(15) Aromí, G.; Gamez, P.; Berzal, P. C.; Driessen, W. L.; Reedijk, J. *Synth. Commun.* **2003**, *33*, 11−18.

(16) Aromí, G.; Gamez, P.; Roubeau, O.; Carrero-Berzal, P.; Kooijman, H.; Spek, A. L.; Driessen, W. L.; Reedijk, J. *Eur. J. Inorg. Chem* **2002**, 1046−1048.

(17) Aromí, G.; Berzal, P. C.; Gamez, P.; Roubeau, O.; Kooijman, H.; Spek, A. L.; Driessen, W. L.; Reedijk, J. *Angew. Chem., Int. Ed.* **2001**, *40*, 3444.

(18) Aromí, G.; Ribas, J.; Gamez, P.; Roubeau, O.; Kooijman, H.; Spek, A. L.; Teat, S.; MacLean, E.; Stoeckli-Evans, H.; Reedijk, J. *Chem.−Eur. J.* **2004**, *10*, 6476−6488.

(19) Aromí, G.; Gamez, P.; Boldron, C.; Kooijman, H.; Spek, A. L.; Reedijk, J. *Eur. J. Inorg. Chem.* **2006**, 1940−1944.

(20) Benton, F. L.; Dillon, T. E. *J. Am. Chem. Soc.* **1942**, *64*, 1128−1129.

Table 1. Crystallographic Data for Compounds **H_5L**, $[Ni_2(H_3L)_2(py)_4]$ (**1**), $[Co_2(H_3L)_2(py)_4]$ (**2**), $[Mn_4(H_2L)_2(AcO)_2(py)_5]$ (**3**), $[Mn_4(H_2L)_2(AcO)_2(dmf)_4]$ (**4**), and $[Mn_3(HL)_2(py)_6]$ (**5**)

	H_5L	**1**	**2**	**3**	**4**	**5**
formula	$C_{24}H_{18}O_7$	$C_{78}H_{62}N_5Ni_2O_{14}$	$C_{39}H_{28}CoN_3O_7$	$C_{77}H_{61}Mn_4N_5O_{18}$	$C_{64}H_{64.6}Mn_4N_4O_{22.3}$	$C_{85.5}H_{66}Mn_3N_{7.5}O_{14.2}$
fw	418.38	1424.72	709.57	1564.07	1466.00	1591.28
crystal syst	orthorhombic	triclinic	monoclinic	triclinic	monoclinic	triclinic
space group	*Pbcn*	$P\bar{1}$	$P2_1/c$	$P\bar{1}$	$P2_1/c$	$P\bar{1}$
a/Å	13.9229(15)	8.929(2)	12.932(2)	10.8441(10)	15.8846(11)	10.5020(3)
b/Å	8.5263(12)	11.205(2)	9.0376(17)	18.591(2)	15.8321(11)	17.7237(5)
c/Å	32.190(5)	17.579(6)	28.463(5)	20.904(3)	14.0294(10)	19.9453(5)
α/°	90.00	103.625(15)	90.00	85.172(15)	90.00	98.608(2)
β/°	90.00	90.170(15)	92.615(2)	77.893(15)	113.446(2)	94.671(2)
γ/deg	90.00	106.18(2)	90.00	87.872(15)	90.00	91.647(2)
V/Å^3	3821.3(9)	1637.1(8)	3323.1(10)	4105.1(9)	3236.9(4)	3655.34(17)
Z	8	1	4	2	2	2
$\rho_{calcd}{}^{a}$/g cm^{-3}	1.454	1.445	1.418	1.265	1.504	1.446
T/K	150	150	150(2)	150	180(2)	150(2)
crystal shape	block	plate	plate	block	plate	rod
color	yellow	pale green	blue	pale orange	yellow	brown
dimens/mm	0.08 ×0.06 × 0.01	0.03 × 0.10 × 0.20	0.08 × 0.06 × 0.01	0.05 × 0.18 × 0.35	0.14 × 0.10 × 0.03	0.08 × 0.01 × 0.01
unique data	3410	7480	4937	14 832	9794	21 645
unique data with $I > 2\sigma(I)$	2302	5679	3855	11 825	7410	16 334
R1, wR2^{b}	0.0468, 0.1254	0.0386, 0.0877	0.0486, 0.1140	0.0443, 0.0407	0.0384, 0.0901	0.0554, 0.1460

[a] For **3**, excluding disordered solvent contribution. [b] $R1 = \Sigma ||F_o| - |F_c||/\Sigma |F_o|$, $wR2 = [(\Sigma w(F_o^2 - F_c^2)^2 / \Sigma w F_o^4)]^{1/2}$.

form present in solution. One of these forms was trapped in the solid state, and its structure was determined by X-ray crystallography (see below). The ^1H NMR spectrum (see Supporting Information) was consistent with the molecular symmetry in the solid state and could be assigned with help of COSY experiments and, for the protons involved in the keto−enolic processes, assuming the correlation predicted for resonance-assisted hydrogen-bonded (RAHB) systems,[21] between the [O−H···O] distance and the chemical shift.

The ability of the heptadentate donor **H_5L** to assemble transition metals into linear arrays was investigated with various metallic salts, always using 2 equiv of metallic ion per ligand. The reaction in pyridine with $Ni(AcO)_2$ produced crystals of $[Ni_2(H_3L)_2(py)_4]$ (**1**). This complex contains only two separated metals and results from the sole deprotonation of the ligand at the 1,3-diketone moieties, the phenol groups remaining protonated. The latter are certainly stabilized by internal hydrogen bonds, the acetate group not being a sufficiently strong base to subtract them. Indeed, the use of stronger bases led to precipitates with a probable higher metal content, and attempts to crystallize these compounds are currently in progress. On the other hand, changing the ligand-to-metal ratio only does not lead to any identifiable change in reactivity. Similarly, the reaction with $Co(AcO)_2$ generated the complex $[Co_2(H_3L)_2(py)_4]$ (**2**), which could be characterized by X-ray crystallography, using a synchrotron radiation source. These simple processes are perfectly described by eq 1 (with M = Ni^{II} or Co^{II})

$$2M(AcO)_2 + 2\mathbf{H_5L} + 4py \rightarrow [M_2(H_3L)_2(py)_4] + 4AcOH \quad (1)$$

The same reaction was performed with $Mn(AcO)_2$, and surprisingly, this resulted in a completely distinct product, with formula $[Mn_4(H_2L)_2(AcO)_2(py)_5]$ (**3**), also during the course of a clean transformation

$$4Mn(AcO)_2 + 2\mathbf{H_5L} + 5py \rightarrow [Mn_4(H_2L)_2(AcO)_2(py)_5] + 6AcOH \quad (2)$$

The major differences between this manganese complex and the previous compounds are the nuclearity, the fact that **3** incorporates the ligand carboxylate, and the higher degree of deprotonation of the polydentate ligand **H_5L**. The reasons for such differences in reactivity are difficult to appraise. A possible explanation is the ability of Mn^{II} centers to adapt to more distorted coordination environments, as compared with Co^{II} and Ni^{II} and as can be seen with the two analogous complexes $[M_3(HL1)_3]$ (M = Mn^{II}, Co^{II})[17,22] where H_3L1 is a ligand similar to **H_5L**, without the external OH groups. Important structural disparities between the product with Mn^{II} vs the products with Co^{II} and Ni^{II} were already observed with H_3L1 and explained in terms of subtle differences of crystal field stabilization energies.[16,22] The differences in reactivity, however, do not seem to be associated to the ability of Mn to exist in different oxidation states, since the oxidation of Mn is only observed at latter stages (see below), after isolation of the Mn^{II} complexes. When the reaction to prepare **3** was performed in DMF, the analogous cluster $[Mn_4(H_2L)_2(AcO)_2(dmf)_4]$ (**4**) was obtained, which could be characterized by single-crystal X-ray diffraction (synchrotron source). Unfortunately, no product could be isolated when performing the reaction in a noncoordinating solvent. All the above complexes were obtained in crystalline form by layering the corresponding reaction mixtures with Et_2O. A quite remarkable process was observed when the system producing crystals of **3** was left unperturbed for a few weeks.

---

(21) Bertolasi, V.; Gilli, P.; Ferretti, V.; Gilli, G. *J. Chem. Soc., Perkin Trans.* **1997**, 945−952.

(22) Aromí, G.; Stoeckli-Evans, H.; Teat, S. J.; Cano, J.; Ribas, J. *J. Mater. Chem.* **2006**, *16*, 2635−2644.

Table 2. Selected Interatomic Distances (Å) for Compound $\mathbf{H_5L}$

O(1)−C(22)	1.354(2)	C(41)−C(43)	1.400(3)
O(2)−C(20)	1.234(2)	C(41)−C(50)	1.479(2)
O(3)−C(30)	1.237(2)	C(42)−C(44)	1.392(3)
O(4)−C(40)	1.341(2)	C(43)−C(45)	1.381(3)
O(5)−C(50)	1.331(2)	C(44)−C(45)	1.372(3)
O(6)−C(60)	1.277(2)	C(50)−C(51)	1.365(3)
O(7)−C(62)	1.359(2)	C(51)−C(60)	1.437(2)
C(20)−C(21)	1.468(3)	C(60)−C(61)	1.470(3)
C(20)−C(31)	1.521(3)	C(61)−C(62)	1.413(2)
C(21)−C(22)	1.415(3)	C(61)−C(66)	1.400(3)
C(21)−C(26)	1.403(3)	C(62)−C(63)	1.387(3)
C(22)−C(23)	1.388(3)	C(63)−C(64)	1.371(3)
C(23)−C(24)	1.365(3)	C(64)−C(65)	1.389(3)
C(24)−C(25)	1.394(3)	C(65)−C(66)	1.378(3)
C(25)−C(26)	1.372(3)	O(1)−H···(2)	2.578(2)
C(30)−C(31)	1.508(3)	O(3)−H···O(4)	2.533(2)
C(30)−C(42)	1.467(3)	O(5)−H···O(6)	2.488(2)
C(40)−C(41)	1.408(3)	O(6)−H···O(7)	2.536(2)
C(40)−C(42)	1.422(2)		

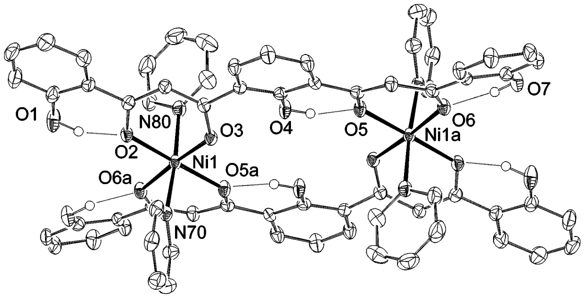

Figure 2. ORTEP representation at 50% probability level of $[Ni_2(H_3L)_2(py)_4]$ (**1**). Only hydroxyl H atoms are shown. Intramolecular hydrogen bonds are shown as dashed lines. This representation also describes accurately the structure of $[Co_2(H_3L)_2(py)_4]$ (**2**), if the metal label is changed accordingly.

Scheme 2

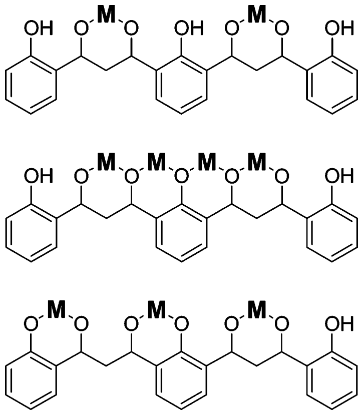

During that period, these crystals slowly redissolved with concomitant deposition of dark brown crystals of a new product. This reaction took place to completion, and thus, a new complex could be isolated, whose formula, $[Mn_3(HL)_2(py)_6]$ (**5**), was established by synchrotron X-ray diffraction. Complex **5** comprises one Mn^{II} and two Mn^{III} ions, thus representing an increase of the average oxidation state of the metals from +2 to +2.7. In addition, the deprotonation degree of the polydentate ligand has risen from three ionized protons to four through the transformation of complex **3** to **5**. After identification of the new complex **5**, the preparation from its components was accomplished in pyridine through the comproportionation between Mn^{VII} and Mn^{II} in the appropriate ratio to give an $[Mn^{III}{}_2Mn^{II}]$ product, as described in eq 3. This was verified by infrared spectroscopy, elemental analysis, and magnetic measurements.

$$Bu_4NMnO_4 + {}^{13}/_2Mn(AcO)_2 + 5\mathbf{H_5L} + 6py \rightarrow {}^{15}/_6[Mn_3(HL)_2(py)_6] + Bu_4NAcO + 12AcOH + 4H_2O \quad (3)$$

Description of the Structures. Representations of the molecular structures of compounds $\mathbf{H_5L}$, **1**, **2**, **3**, **4**, and **5** are depicted in Figures 1−6. Crystallographic data are reported in Table 1, whereas selected interatomic distances and angles are in Tables 2−4 and in the captions of Figures 3 and 5.

$\mathbf{H_5L.}$ The single-crystal X-ray diffraction of this molecule reveals that in the solid state it exhibits one of the β-diketone groups in the enolic form (O5, O6), whereas the other is present as the biscarbonyl tautomer (O2, O3). This is reflected by the positions of the relevant hydrogen atoms and by the various C−O bond distances (Table 2). The simultaneous presence of both forms within the same molecule is extremely rare, and we are aware of only one previous example, corresponding to a cyclic polyketide lactone, where the strain imposed by the molecular structure may enforce the mixed tautomeric display.[23] Compound $\mathbf{H_5L}$ is a very rich example of the manifestation of RAHB,[21] by which the existence of π-delocalization within a heterodienic cyclic chain, [O═C−C−C═O−H···], and intramolecular hydrogen bonding within such a cycle mutually reinforce one other in a synergistic manner. This translates into very short O···O distances, d(O···O) (Table 2). In the molecule $\mathbf{H_5L}$, this phenomenon occurs four times, three times within the 2-hydroxybenzoketone moieties and once as a 1,3-diketone (or ketoenol). The four hydrogen atoms involved in these interactions have been located crystallographically. Among all the possibilities, this distribution of internal hydrogen bonds leads to the most stable combination of tautomers, and it is retained in $CHCl_3$ solution, as shown by ^1H NMR spectroscopy. The correlation found to exist between d(O···O) and the ^1H NMR chemical shift of the proton involved in the corresponding RAHB was used to help assign the spectrum of $\mathbf{H_5L}$ (see Supporting Information). All the atoms of the molecule (except the methylenic H atoms) are essentially contained in either of two planes that form a dihedral angle of approximately 76° and share one atom, C30. A complicated network of π−π stacking interactions maintains the molecules in the solid state.

$\mathbf{[Ni_2(H_3L)_2(py)_4]}$ **(1).** Complex **1** (Figure 2) is a dinuclear complex of Ni^{II} ions bridged by two crystallographically equivalent bis-deprotonated $\mathbf{H_5L}$ ligands (i.e., in the H_3L^{2-} form; Scheme 2, top). The latter have lost their protons from the 1,3-diketone moieties, which now function as chelates at the equatorial positions of the pseudo-octahedral metal ions, their axial sites being occupied by solvate pyridine ligands. The phenol protons remain at their original locations, being part of intramolecular hydrogen bonds as observed in the free ligand (see above), although H_3L^{2-} has varied its

---

(23) Tatsuta, K.; Chino, M.; Kojima, N.; Shinojima, S.; Nakata, M.; Morooka, M.; Ohba, S. *Tetrahedron Lett.* **1993**, *34*, 4957−4960.

Table 3. Selected Interatomic Distances (Å) and Angles (deg) for Complexes $[M_2(H_3L)_2(py)_4]$ (M = Ni, **1**; Co, **2**) in the **1**/**2** Format

M(1)−O(2)	2.0120(14)/2.040(2)
M(1)−O(3)	2.0241(14)/2.045(2)
M(1)−N(70)	2.1073(17)/2.167(3)
M(1)−N(80)	2.1504(18)/2.202(3)
M(1)−O(5)^a	1.9862(14)/2.013(2)
M(1)−O(6)^a	2.0138(14)/2.057(3)
O(2)−M(1)−O(3)	87.13(5)/85.43(9)
O(2)−M(1)−N(70)	87.64(6)/90.03(10)
O(2)−M(1)−N(80)	90.42(6)/88.72(10)
O(2)−M(1)−O(5)^a	175.93(6)/177.64(8)
O(2)−M(1)−O(6)^a	93.40(5)/93.59(9)
O(3)−M(1)−N(70)	91.38(6)/92.65(9)
O(3)−M(1)−N(80)	92.66(6)/88.56(9)
O(3)−M(1)−O(5)^a	90.64(5)/92.37(9)
O(3)−M(1)−O(6)^a	178.73(5)/176.12(9)
N(70)−M(1)−N(80)	175.42(6)/178.18(10)
N(70)−M(1)−O(5)^a	89.02(6)/90.91(10)
N(70)−M(1)−O(6)^a	89.79(6)/91.11(10)
N(80)−M(1)−O(5)^a	93.09(6)/90.39(10)
N(80)−M(1)−O(6)^a	86.19(6)/87.66(10)
O(5)a−M(1)−O(6)^a	88.89(5)/88.56(9)

^{a} The $[1 - x, 1 - y, -z]$ symmetry operation was utilized.

conformation upon coordination with respect to solid $\mathbf{H_5L}$. The intramolecular $Ni^{II}\cdots Ni^{II}$ distance is 7.714(3) Å whereas the shortest intermolecular metal−metal separation is 8.929(3) Å. Other selected interatomic distances and angles are collected in Table 3. The degree of coplanarity of the ligand H_3L^{2-} can be gauged by the angle formed by the idealized chelate rings. For complex **1**, this angle is 20.01(6)°. The packing in the solid state occurs because of interactions between the pyridine ligands from different molecules and as a consequence of mutual interdigitation. In addition to complex **1**, the unit cell contains one molecule of uncoordinated pyridine per dinuclear entity, establishing $\pi-\pi$ interactions with one pyridine ligand.

$\mathbf{[Co_2(H_3L)_2(py)_4]}$ **(2).** Complex **2** (Figure 2) is the Co^{II} analogue of **1**. This similarity in reactivity between Ni^{II} and Co^{II} is often encountered,[24] and it has been observed with ligand systems very similar to $\mathbf{H_5L}$.[16,22] The intermetallic distances here are 7.807 (intramolecular) and 9.038 Å (intermolecular). The packing between the molecules occurs through various weak van der Waals interactions involving aromatic rings but in a different manner than in complex **1**. In this case, there is no interdigitation between the pyridine rings of different molecules, and the rings of H_3L^{2-} also participate in these interactions. This may explain the differences in conformation of the polydentate ligand when comparing **1** with **2**. For complex **2**, the ligand is more removed from planarity; the angle between idealized chelate rings is 34.0(1)°. The uncoordinated pyridine ligand present in complex **1**, not observed in **2**, may also explain these differences in part.

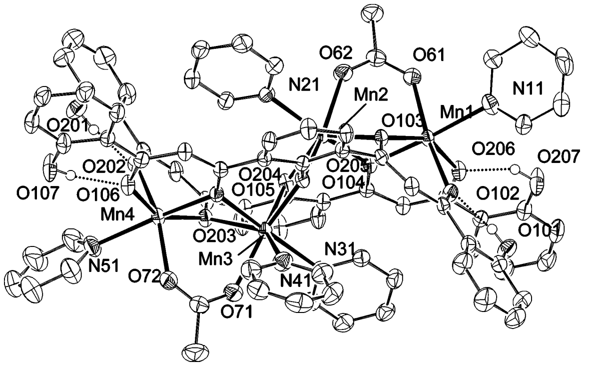

Figure 3. ORTEP representation at 50% probability level of $[Mn_4(H_2L)_2(AcO)_2(py)_5]$ (**3**). Only hydroxyl H atoms are shown. Intramolecular hydrogen bonds are shown as dashed lines. Ranges of selected interatomic distances (Å) and angles (deg): Mn−O(AcO), 2.120(2)−2.152(2); Mn−O(H_2L), 2.066(2)− 2.403(2); Mn−N, 2.266(2)−2.488(2); Mn1···Mn2, 3.2876(6); Mn2···Mn3, 3.4950(7); Mn3···Mn4, 3.3502(6); Mn1···Mn3, 5.8984(9); Mn2···Mn4, 5.7526(9); Mn1···Mn4, 8.8046(13); Mn1−Mn2−Mn3, 120.80(2); Mn2−Mn3−Mn4, 114.35(2); Mn1−Mn2−Mn3−Mn4, −176.32(2); O107−H···O106, 2.513(2); O207−H···O206, 2.500(2); O101−H···O102, 2.501(2); O201−H···O202, 2.495(2).

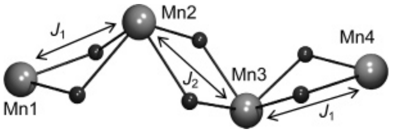

Figure 4. POV-ray representation of the core of $[Mn_4(H_2L)_2(AcO)_2(py)_5]$ (**3**), showing the spin-coupling scheme used to model its magnetic behavior.

$\mathbf{[Mn_4(H_2L)_2(AcO)_2(py)_5]}$ **(3).** Complex **3** (Figure 3) is a tetranuclear cluster of Mn^{II} with a $[Mn_4O_6]$ zigzag linear core (Figure 4). This arrangement is built up by the action of two H_2L^{3-} ligands located opposite to each other and running along the chain, each engaging its central phenolate and both 1,3-diketonate moieties for coordination, thereby chelating and bridging the metals through four adjacent [O−C−C−C−O] coordination pockets (Scheme 2, middle). The external phenol moieties of the ligands are not involved in coordination and retain their protons, which form intramolecular hydrogen bonds as in complexes **1** and **2**. Additional bridging within the cluster is ensured by two *syn,syn*-OAc^- ligands, supporting the Mn_{1-2} and Mn_{3-4} pairs, respectively. The central pair is in turn bridged only by two alkoxide-type oxygen atoms. Terminal ligation is completed by five pyridine ligands, one on each metal except for Mn3, which is bound to two such molecules and is therefore heptacoordinated. The remaining manganese ions are pseudo-octahedral. The bond distances to the metals (see Figure 3 caption) agree well with the oxidation state of +2, which is consistent with the electroneutrality of the molecule. The intramolecular metal−metal separations are (in Å) 3.2876(6) (Mn_{1-2}), 3.4950(7) (Mn_{2-3}), 3.3502(6) (Mn_{3-4}), 5.7526(9) (Mn_{2-4}), 5.8984(9) (Mn_{3-1}), and 8.8046(13) (Mn_{1-4}). The angles of the “zigzag” can be gauged with the parameters of Mn1−Mn2−Mn3 (120.80(2)°) and Mn2−Mn3−Mn4 (114.35(2)°). Interestingly, the H_2L^{3-} ligand is found here in a conformation highly reminiscent of its free form in the solid state. The moderate degree of flexibility of the ligand, together with its linear array of O-donors, facilitates the formation of this interesting $[Mn_4O_6]$ architecture. The improper torsion angle formed by the four Mn ions within the molecule is −176.32(2)°, with these atoms thus being close to lying within the same plane. Tetranuclear manganese/oxo aggregates have been perceived as potential models for the oxygen-evolving center of photosystem II.[25] Of the many published examples, relatively few consist of linear arrays

---

(24) Aromí, G.; Batsanov, A. S.; Christian, P.; Helliwell, M.; Roubeau, O.; Timco, G. A.; Winpenny, R. E. P. *Dalton Trans.* **2003**, 4466−4471.

Scheme 3

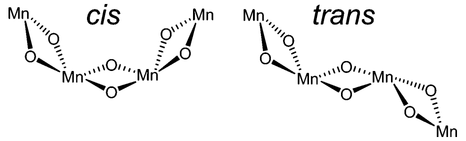

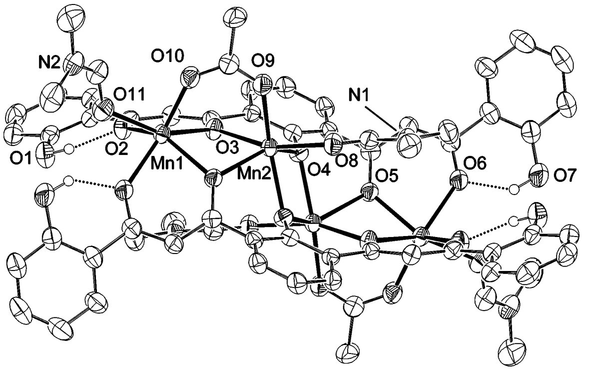

Figure 5. ORTEP representation at 50% probability level of $[Mn_4(H_2L)_2(AcO)_2(dmf)_4]$ (**4**). Only hydroxyl H atoms are shown. Intramolecular hydrogen bonds are shown as dashed lines. Ranges of selected interatomic distances (Å) and angles (deg): Mn−O(AcO), 2.092(2)−2.119(1); Mn−O(H_2L), 2.082(1) −2.274(1); Mn−O(dmf), 2.185(1)−2.260(2); Mn1⋯Mn2, 3.3182(5); Mn2⋯Mn2a, 3.3877(5); Mn1⋯Mn2a, 5.8618(6); Mn1⋯Mn1a, 8.9031(8); Mn1−Mn2−Mn2a, 121.88(1); Mn1−Mn2−Mn2a−Mn1a, 180; O1−H⋯O2, 2.605(2); O7−H⋯O6, 2.544(2).

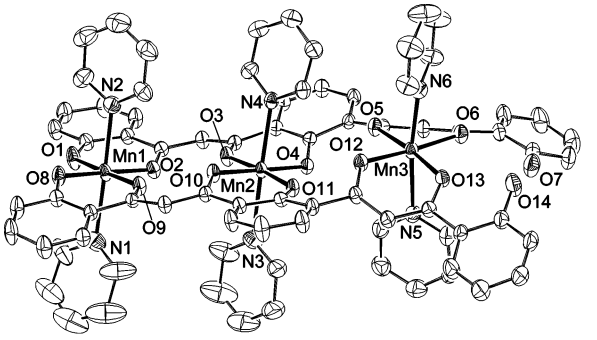

Figure 6. ORTEP representation at 50% probability level of $[Mn_3(HL)_2(py)_6]$ (**5**). H atoms are not shown.

of fused $[Mn_2(\mu\text{-}O)_2]$ moieties as in **3**.[26−30] The latter is the first Mn^{II} example where the oxo-bridged dimers are in relative trans configuration (zigzag) as opposed to cis (Scheme 3). The trans configuration is, however, for other metals, known to coordination chemistry.[31−34] The packing diagram of this compound does not reveal any special intermolecular interactions other than a plethora of van der Waals contacts (not shown).

$[Mn_4(H_2L)_2(AcO)_2(dmf)_4]$ (4). Complex **4** (Figure 5) is analogous to **3** with dmf terminal ligands instead of pyridine. Now, each manganese ion is bound to one solvate ligand and all metal centers are thus octahedral. As a result, the compound now displays crystallographic inversion symmetry. The remaining structural parameters (Figure 5 caption) are essentially the same as in **3**, with the following intermetallic distances (in Å) of 3.3182(5) (Mn_{1-2}), 3.3877(5) (Mn_{2-2a}), 5.8618(6) (Mn_{1-2a}), and 8.9031(8) (Mn_{1-1a}). The zigzag and torsion angles are 121.88(1)° (Mn1−Mn2−Mn2a) and 180°, respectively (the latter by virtue of the crystallographic symmetry). No remarkable features are observed on the packing diagram of this complex.

$[Mn_3(HL)_2(py)_6]$ (5). The structure of **5** (Figure 6) comprises a mixed-valence trinuclear $[Mn^{III}{}_2Mn^{II}]$ complex supported by two HL^{4-} ligands, one on each side of the chain, which balance the metallic charges. The O-donors of these ligands occupy all the equatorial positions of the metals as chelates, the axial sites being saturated by pyridine ligands. The ligand HL^{4-} is found here at almost its highest possible level of deprotonation, coordinating the metals in an asymmetric manner, by using three nonadjacent coordination pockets (Scheme 2, bottom). This comes about through the involvement of two phenoxide groups and β-diketonate moieties per ligand. The third phenol moiety of each ligand retains its proton, and both groups are found in front of each other at the same end of the molecule. The Mn^{III} centers are identified within this complex (Mn1 and Mn2) by the presence of Jahn−Teller elongation axes (corresponding to the bonds with pyridines). On the other hand, the bond distances around Mn3 (Table 4) are consistent with the assignment of the oxidation state +2. The intermetallic distances in this complex are (in Å) 5.2463 (Mn_{1-2}), 5.1553 (Mn_{2-3}), and 10.3819 (Mn_{1-3}), whereas the angle of Mn1−Mn2−Mn3 is 172.92°. There are other linear trinuclear complexes in the literature, featuring mixtures of Mn ions in the oxidation states of +2 and +3, either as $[Mn^{III}Mn^{II}Mn^{III}]$[35,36] or as $[Mn^{II}Mn^{III}Mn^{II}]$,[37,38] the former being about twice as numerous as the latter. All these complexes are, however, symmetric, thus featuring the unique Mn ion as the central atom of the array. Complex **5** is the first asymmetric compound of this category and thus the only one to exhibit the sequence $[Mn^{III}Mn^{III}Mn^{II}]$. This has interesting implications with regard to the magnetic properties of this molecule (see below). The molecules of complex **5** are cemented within the crystal by means of van der Waals interactions as well as a network of $\pi-\pi$ bonds established

---

(25) Mukhopadhyay, S.; Mandal, S. K.; Bhaduri, S.; Armstrong, W. H. *Chem. Rev.* **2004**, *104*, 3981−4026.

(26) Dave, B. C.; Czernuszewicz, R. S. *New J. Chem.* **1994**, *18*, 149−155.

(27) Philouze, C.; Blondin, G.; Girerd, J. J.; Guilhem, J.; Pascard, C.; Lexa, D. *J. Am. Chem. Soc.* **1994**, *116*, 8557−8565.

(28) Yoo, J.; Yamaguchi, A.; Nakano, M.; Krzystek, J.; Streib, W. E.; Brunel, L. C.; Ishimoto, H.; Christou, G.; Hendrickson, D. N. *Inorg. Chem.* **2001**, *40*, 4604−4616.

(29) Jeffery, J. C.; Thornton, P.; Ward, M. D. *Inorg. Chem.* **1994**, *33*, 3612−3615.

(30) Bardwell, D. A.; Jeffery, J. C.; Ward, M. D. *J. Chem. Soc., Dalton. Trans.* **1995**, 3071−3080.

(31) Kemmitt, T.; Gainsford, G. J.; Al-Salim, N. I. *Acta Crystallogr., Sect. C: Cryst. Struct. Commun.* **2004**, *60*, M42−M43.

(32) Dey, M.; Pao, C. P.; Saarenketo, P. K.; Rissanen, K. *Inorg. Chem. Commun.* **2002**, *5*, 380−383.

(33) Burger, J.; Klufers, P. *Z. Anorg. Allg. Chem.* **1997**, *623*, 1547−1554.

(34) Cotton, F. A.; Elder, R. C. *Inorg. Chem.* **1965**, *4*, 1145−1151.

(35) Kitajima, N.; Osawa, M.; Imai, S.; Fujisawa, K.; Morooka, Y.; Heerwegh, K.; Reed, C. A.; Boyd, P. D. W. *Inorg. Chem.* **1994**, *33*, 4613−4614.

(36) Tangoulis, V.; Malamatari, D. A.; Spyroulias, G. A.; Raptopoulou, C. P.; Terzis, A.; Kessissoglou, D. P. *Inorg. Chem.* **2000**, *39*, 2621−2630.

(37) Liu, J. C.; Xu, Y.; Duan, C. Y.; Wang, S. L.; Liao, F. L.; Zhuang, J. Z.; You, X. Z. *Inorg. Chim. Acta* **1999**, *295*, 229−233.

(38) Tan, X. S.; Sun, J.; Hu, C. H.; Fu, D. G.; Xiang, D. F.; Zheng, P. J.; Tang, W. X. *Inorg. Chim. Acta* **1997**, *257*, 203−210.

Table 4. Selected Interatomic Distances (Å) and Angles (deg) for Complex $[Mn_3(HL)_2(py)_6]$ (**5**)

Mn1−O1	1.876(2)	O9−Mn1−N1	90.20(8)
Mn1−O2	1.916(2)	O9−Mn1−N2	89.27(7)
Mn1−O8	1.886(2)	N1−Mn1−N2	177.24(7)
Mn1−O9	1.893(1)	O3−Mn2−O4	89.53(6)
Mn1−N1	2.331(2)	O3−Mn2−O10	87.55(6)
Mn1−N2	2.294(2)	O3−Mn2−O11	174.96(7)
Mn2−O3	1.889(1)	O3−Mn2−N3	88.67(7)
Mn2−O4	1.883(1)	O3−Mn2−N4	90.58(7)
Mn2−O10	1.894(2)	O4−Mn2−O10	177.08(6)
Mn2−O11	1.872(1)	O4−Mn2−O11	92.87(6)
Mn2−N3	2.378(2)	O4−Mn2−N3	90.52(7)
Mn2−N4	2.352(2)	O4−Mn2−N4	86.77(6)
Mn3−O5	2.109(2)	O10−Mn2−O11	90.04(6)
Mn3−O6	2.144(2)	O10−Mn2−N3	89.37(7)
Mn3−O12	2.112(2)	O10−Mn2−N4	93.97(7)
Mn3−O13	2.150(2)	O11−Mn2−N3	86.88(7)
Mn3−N5	2.321(2)	O11−Mn2−N4	93.97(7)
Mn3−N6	2.266(2)	N3−Mn2−N4	177.19(7)
Mn1···Mn2	5.2462(4)	O5−Mn3−O6	83.82(6)
Mn2···Mn3	5.1547(4)	O5−Mn3−O12	93.91(6)
Mn1···Mn3	10.3811(5)	O5−Mn3−O13	173.68(6)
O6−O7	2.555(3)	O5−Mn3−N5	91.14(7)
O13−O14	2.503(2)	O5−Mn3−N6	94.71(7)
O1−Mn1−O2	89.72(7)	O6−Mn3−O12	176.46(6)
O1−Mn1−O8	92.62(7)	O6−Mn3−O13	101.84(6)
O1−Mn1−O9	176.61(7)	O6−Mn3−N5	86.76(7)
O1−Mn1−N1	90.78(9)	O6−Mn3−N6	88.92(7)
O1−Mn1−N2	89.90(8)	O12−Mn3−O13	80.56(6)
O2−Mn1−O8	177.64(6)	O12−Mn3−N5	96.02(7)
O2−Mn1−O9	87.00(6)	O12−Mn3−N6	88.24(7)
O2−Mn1−N1	92.63(7)	O13−Mn3−N5	86.43(7)
O2−Mn1−N2	90.05(7)	O13−Mn3−N6	88.24(7)
O8−Mn1−O9	90.67(6)	N5−Mn3−N6	172.31(7)
O8−Mn1−N1	87.03(8)	Mn1−Mn2−Mn3	172.92(1)
O8−Mn1−N2	90.27(8)		

Table 5. CShMs of Coordination Polyhedra within Complexes $[M_2(H_3L)_2(py)_4]$ (M = Ni, **1**; Co, **2**), $[Mn_4(H_2L)_2(AcO)_2(py)_5]$ (**3**), $[Mn_4(H_2L)_2(AcO)_2(dmf)_4]$ (**4**), and $[Mn_3(HL)_2(py)_6]$ (**5**)

Complexes **1**−**5**

ion (complex)	dist to OC[a]	dist to TRP[b]
Ni1 (**1**)	0.20	14.85
Co1 (**2**)	0.19	15.55
Mn1 (**3**)	3.08	7.45
Mn2 (**3**)	8.92	2.49
Mn4 (**3**)	3.89	6.29
“Mn3” (**3**)[c]	12.15	2.32
Mn1 (**4**)	10.59	1.87
Mn2 (**4**)	6.92	3.51
Mn1 (**5**)	1.01	16.48
Mn2 (**5**)	1.31	16.62
Mn3 (**5**)	0.74	12.59

Mn3 of Complex **3** (Heptacoordinated)

dist to PBPY[d]	dist to OCF[e]	dist to TPRS[f]
3.98	2.23	1.10

[a] OC = octahedron. [b] TRP = trigonal prism. [c] Measures of Mn3 after removing N41. [d] PBPY = pentagonal bipyramid. [e] OCF = face-capped octahedron. [f] TPRS = side-face-capped trigonal prism.

between the pyridine ligands from different molecules, along the *b*-axis (see Suppporting Information Figure S1)

Continuous Shape Measures (CShMs). The dramatic difference in reactivity toward **H_5L** exhibited by Co^{II} and Ni^{II} with respect to Mn^{II} is ascribed to the flexibility of the latter to adopt various coordination geometries without significant changes of crystal field energy, in contrast to that of the other two ions, which are more restricted to certain geometries. Discussion of this and other aspects dependent on coordination geometries can be made more precisely in light of the accurate description of the coordination environment around the metals delivered by CShMs.[39,40] These measures are normalized “distances” (in a scale that goes from 0 to 100) with respect to ideal shapes of the polyhedra formed by a metal and the atoms of its first coordination sphere. In the case of six-coordination, the distances of the different chromophores to the regular octahedron (OC) and the ideal trigonal prism (TPR) will be calculated.[39] The only case of heptacoordination encountered here (within complex $[Mn_4(H_2L)_2(AcO)_2(py)_5]$) will be compared to the pentagonal bipyramid (PBPY), the face-capped octahedron (OCF), and the side-face-capped trigonal prism (TRPS).[40] The results of these measures are summarized in Table 5. These calculations show that the Ni^{II} and Co^{II} ions in complexes **1** and **2**, respectively, describe almost perfect regular octahedra (with CShM distances to OC of 0.20 and 0.19, respectively) and are consequently far from being the ideal trigonal prism (distances to TRP of 14.85 and 15.85; note that the distance between the perfect polyhedra OC and TRP is calculated as 16.73). By contrast, the formation of complexes **3** and **4** requires a severe distortion from the octahedral geometry (Mn1, Mn4 in **3**) or coordination arrangements close to the trigonal prism (see Table 5). In fact, Mn2 in **3** and Mn1 in **4** have been calculated to be very close to ideal TRP (measures, in the TRP/OC format, of 2.49/8.92 and 1.87/10.59, respectively). In addition, one Mn^{II} ion in **3** (Mn3) displays seven-coordination; CShMs have shown that the geometry of this center is best described as a trigonal prism capped on one of its side faces (distance to TRPS; 1.10). Indeed, if the donor atom capping the prism (N41) is removed, the remaining shape is an almost perfect trigonal prism (with TRP/OC distances of 2.32/12.15). The three manganese atoms of complex **5** display shapes very near perfect octahedra (Table 5). Interestingly, the Mn^{II} (Mn3) center is closer to the ideal polyhedron than the Mn^{III} chromophores, which reflects the tetragonal elongation caused by the Jahn−Teller distortion on the latter.

Magnetic Properties. The magnetic properties of the tetranuclear and trinuclear complexes of **3** and **5** were examined by bulk magnetization measurements and by X-band (∼9.7 GHz) electron paramagnetic resonance (EPR). Preliminary high frequency (50−400 GHz) EPR experiments were also performed. The magnetometric behavior of **3** has been previously communicated[41] and will only be briefly discussed here.

The $\chi_M T$ vs T plot for **3** (See Supporting Information Figure S2, where χ_M is the molar paramagnetic susceptibility) decreases from a value of 18.43 cm^3 K mol^{-1} at room temperature to 1.22 cm^3 K mol^{-1} near 2 K, indicating dominance of intramolecular antiferromagnetic interactions.

---

(39) Alvarez, S.; Avnir, D.; Llunell, M.; Pinsky, M. *New J. Chem.* **2002**, *26*, 996−1009.

(40) Casanova, D.; Alemany, P.; Bofill, J. M.; Alvarez, S. *Chem.*−*Eur. J.* **2003**, *9*, 1281−1295.

(41) Aromí, G.; Gamez, G.; Boldron, C.; Kooijman, H.; Spek, A. L.; Reedijk, J. *Eur. J. Inorg. Chem.* **2006**, 1940−1944.

These data were fitted using the program CLUMAG[42] by diagonalization of the spin Hamiltonian $H = -2J_1(S_1S_2 + S_3S_4) -2J_2(S_2S_3)$, where $S_i = {}^5/_2$, and by using the numbering scheme for the spins given in Figure 4. A Hamiltonian involving interactions between nonadjacent ions was not used to avoid overparametrization of the fit. Two sets of parameters gave a good fit of the data, both of which predicted dominant antiferromagnetic coupling leading to an $S = 0$ ground state taking place within the Mn_{1-2} and Mn_{3-4} pairs, while giving either weak ferro- or antiferromagnetic coupling for the interaction between Mn2 and Mn3. The fit that produced a better error factor was the second, yielding the parameters of $J_1 = -1.13$ cm^{-1}, $J_2 = -0.43$ cm^{-1}, and $g = 2.08$.[43] The value of g is only slightly larger than expected. However, this value must be taken with caution, since this parameter is the most affected by errors in the molecular weight used for treatment of the magnetic data. These parameters confirm that the coupling is very weak. This is due to a large extent to the distortion in coordination environment of the Mn^{II} ions, which reduces the efficiency of the overlap between magnetic orbitals. The coupling described by J_1 has the same sign as those of previously reported systems showing the same type of connection between Mn^{II} ions (one acetate and two alkoxide ligands).[44,45] The Mn2···Mn3 pair is connected only by two alkoxide oxygen atoms, and thus, few magnetic orbitals participate in the exchange, which together with the distortion of the coordination geometry, leads to even weaker coupling. The systems in the literature exhibiting this coupled moiety have shown either type of interaction and are always very weak.[29,46−49]

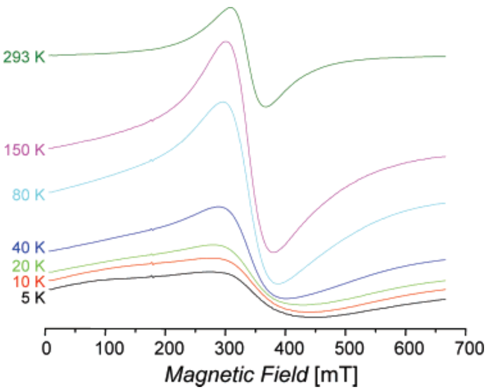

Figure 7. X-band (9.717 GHz) EPR spectra of $[Mn_4(H_2L)_2(AcO)_2(py)_5]$ (**3**) at varying temperatures. Microwave power, 0.2 W (−30 dB); modulation amplitude, 10 mT. The narrow line at 178 mT originates from the dielectric resonator.

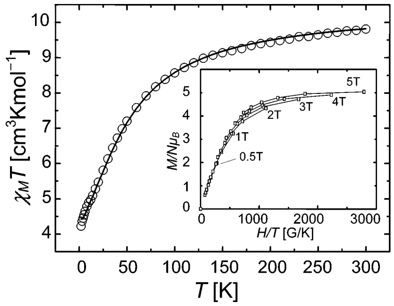

Figure 8. $\chi_M T$ vs T plot of $[Mn_3(HL)_2(py)_6]$ (**5**). The solid line is a fit to the experimental data. The inset displays isofield reduced magnetization lines at different fields.

X-band EPR spectra of complex **3** collected at several temperatures are shown in Figure 7. At low temperature (5 K) the spectrum is asymmetric and shows multiple components hidden under a broad envelope, in particular a shoulder appearing on the low-field side of the spectrum. This feature consistently reappears at high frequencies (not shown) and is thus not an artifact. Upon experiencing an increase in temperature, the spectrum becomes progressively symmetric and the line width becomes smaller, assuming a value of about 300 mT at room temperature. However, even at that temperature, it cannot be simulated using a single Gaussian- or Lorentz-shaped curve. The above EPR characteristics are in very good agreement with the magnetization measurements. In particular, EPR qualitatively confirms the small values of the exchange constants J_i, since even at the lowest conveniently reachable temperature (5 K) there is a significant population of the thermally accessible paramagnetic ($S > 0$) excited states. The small J_i values result in a loss of resolution and an inability to spectrally separate the particular states, although the presence of those states can be deduced from the traces of fine structure, in particular, the low-field shoulder observable at low temperatures at any frequency. The temperature behavior of the EPR spectrum closely follows that observed for the magnetic susceptibility, with the intensity of the EPR absorption rising from low temperature to about 100−120 K and then gradually falling off due to the Curie law. Finally, the g value of the room-temperature line is 2.05, which also confirms the magnetic data. High-frequency and field electron paramagnetic resonance (HFEPR) experiments (not shown) have not succeeded in increasing the spectral resolution; thus, only qualitative observations can be reported here.

The plot of $\chi_M T$ vs T for complex **5**, measured at 0.3 T in the 2−300 K range, is shown in Figure 8 and indicates again the predominance of intramolecular antiferromagnetic interactions. The value of $\chi_M T$ at room temperature (9.8 cm^3 K mol^{-1}) is slightly lower than expected for two uncoupled Mn^{III} ions ($S = 2$) and one independent Mn^{II} center ($S = {}^5/_2$) with average $g = 2$ (10.4 cm^3 K mol^{-1}) and diminishes upon cooling to 4.2 cm^3 K mol^{-1} at 2 K. The extent of the antiferromagnetic exchange was assessed by diagonalization using the program CLUMAG,[42] with the exchange model described by the spin Hamiltonian $H = -2J_1S_1S_2 - 2J_2S_2S_3$, where $S_1 = S_2 = 2$ and $S_3 = {}^5/_2$. The best fit (Figure 8, solid line) was achieved for $J_1 = -5.4$ cm^{-1}, $J_2 = -0.4$ cm^{-1},

---

(42) Gatteschi, D.; Pardi, L. *Gazz. Chim. Ital.* **1993**, *123*, 231.

(43) In the previous communication the coupling constants were mistakenly reported using the $H = -\Sigma JS_1S_2$ convention.

(44) Brooker, S.; McKee, V.; Metcalfe, T. *Inorg. Chim. Acta* **1996**, *246*, 171−179.

(45) Zhong, Z. J.; You, X. Z. *Polyhedron* **1994**, *13*, 2157−2161.

(46) Zhang, Y. Z.; Wei, H. Y.; Pan, T.; Wang, Z. M.; Chen, Z. D.; Gao, S. *Angew. Chem., Int. Ed.* **2005**, *44*, 5841−5846.

(47) Mikuriya, M.; Nakadera, K.; Tokii, T. *Inorg. Chim. Acta* **1992**, *194*, 129−131.

(48) Luneau, D.; Savariault, J. M.; Cassoux, P.; Tuchagues, J. P. *J. Chem. Soc., Dalton Trans.* **1988**, 1225−1235.

(49) Chang, H. R.; Larsen, S. K.; Boyd, P. D. W.; Pierpont, C. G.; Hendrickson, D. N. *J. Am. Chem. Soc.* **1988**, *110*, 4565−4576.

and $g = 2.01$. A previously reported dinuclear complex with two Mn^{III} ions bridged in a manner similar to that found in **3** exhibited a coupling constant of -1.48 cm^{-1}.[50] Most likely, the $Mn^{III}\cdots Mn^{III}$ exchange occurs through the π system of the bridging ligands. The fact that the coupling through the $Mn^{III}\cdots Mn^{II}$ pathway (J_2) is 1 order of magnitude smaller than J_1 is probably caused by the disruption of the conjugation occurring along the bridging chain of atoms (because of the rotation around one of the C−C bonds within this chain). The combination of exchange constants is conducive to a total spin ground state of $S_T = {}^5/_2$, with the first excited state ($S_T = {}^3/_2$) located 10 cm^{-1} greater in energy. This is consistent with the topology of the cluster; all previous linear clusters with the same distribution of metal oxidation states are symmetric with a central Mn^{II}; consequently, in these complexes there is only one type of coupling constant between adjacent metals, in contrast with complex **3**. If this constant is ferromagnetic,[51] the compound has $S_T = {}^{13}/_2$, whereas for antiferromagnetic cases, $S_T = {}^3/_2$.[52] Exceptions to this can occur if the interaction between the terminal Mn ions is not negligible and competes with the interaction between first neighbors, resulting in a different ground state.[53] Complex **5** is the first linear mixed-valence $Mn^{II/III}$ trimer with the asymmetric topology $Mn^{III}-Mn^{III}-Mn^{II}$ and is therefore the only one leading to an $S_T = {}^5/_2$ ground state, which is expected here if both interactions are antiferromagnetic. This ground state is in agreement with the results from reduced magnetization measurements (Figure 8, inset), which were performed at variable temperature for various fixed magnetic fields. The curve at the highest field saturates for a value near 5, which is the expected situation for this ground state. The various isofield lines are not exactly superimposable, a situation which may be caused by the presence of zero field splitting (ZFS). This should not be surprising, since this molecule contains two Mn^{III} ions with mutually parallel Jahn−Teller axes, a situation known to favor single-molecule magnet behavior.[54] Reduced magnetization measurements at constant temperature (2 K) and variable field were performed and the curve was fit (Supporting Information, Figure S3) through a numerical procedure based on the full diagonalization of the spin Hamiltonian $H = \beta BgS_T + D(S_{Tz}^2 - S_T(S_T + {}^\circ 1)/3)$ for $S_T = {}^5/_2$ (the remaining terms have the usual values). This procedure yielded the parameters of $g = 2.03$ and $D = +0.4$ cm^{-1}. The appropriateness of the model used for the fitting procedure is supported by the fact that at 2 K and zero field, 99.9% of the molecules lie at the spin ground state. As expected for a positive value of ZFS, ac susceptibility measurements yielded no out-of-phase signal of the magnetic susceptibility at the highest frequency used (1340 Hz) down to 2 K.

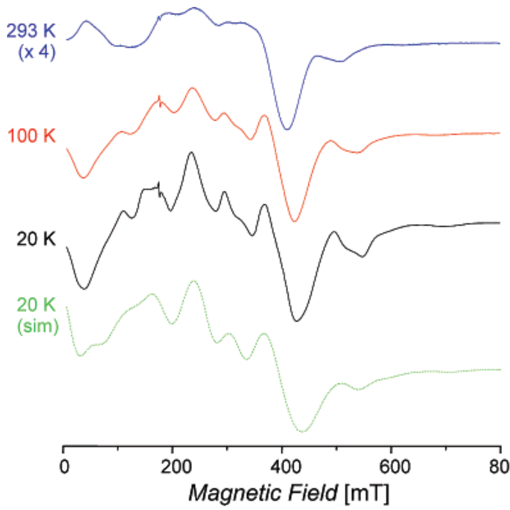

Figure 9. Representative X-band (9.722 GHz) EPR spectra of $[Mn_3(HL)_2(py)_6]$ (**5**) at varying temperatures. Experimental conditions are as in Figure 7.

X-band EPR spectra of complex **5,** shown in Figure 9, are remarkably different from those of complex **3** and display a rich structure at any temperature (at low temperatures (<20 K) the spectra are distorted by fast-passage effects). With the help of preliminary HFEPR experiments (not shown), that structure can be unambiguously ascribed to the zero-field splitting of the ground $S_T = {}^5/_2$ state of the complex. Simulations established the value of the *D* parameter as $+0.085(5)$ cm^{-1}, i.e., typical for mononuclear Mn(II) complexes in the conditions of low symmetry.[55] This value is, almost by a factor of 5, smaller than that obtained from magnetization data ($+0.4$ cm^{-1}). EPR, being a spectroscopic technique, is more accurate than bulk magnetization measurements, and it therefore provides more reliable parameters. The ZFS tensor may be rhombic, although the rhombic parameter *E* used in the simulation of the 20 K spectrum (0.01 cm^{-1}) needs to be re-evaluated at high frequencies. HFEPR also shows other well-defined thermally accessible states that are not observable at low frequencies. It appears that these states are of non-Kramers (integer-spin number) nature, unlike the spin state responsible for the X-band spectra shown in Figure 9. Because of the richness and complexity of HFEPR spectra and phenomena observable in complex **5** in high-frequency and high-field conditions as well as the preliminary status of the HFEPR investigation, we will present those results in a subsequent paper. For the purpose of the current work we may stress the confirmation of the magnetometric results by EPR in terms of the nature of the ground spin state ($S_T = {}^5/_2$) and the presence of sizable zero-field splitting in that state. The appearance of non-Kramers state(s) in the spectra at elevated temperatures can be tentatively explained by the very small coupling constant J_2 between the Mn(II) ion and the two Mn(III) moieties. In effect, this means that complex **5** consists, magnetically

---

(50) Aromí, G.; Gamez, P.; Roubeau, O.; Berzal, P. C.; Kooijman, H.; Spek, A. L.; Driessen, W. L.; Reedijk, J. *Inorg. Chem.* **2002**, *41*, 3673−3683.

(51) Scott, R. T. W.; Parsons, S.; Murugesu, M.; Wernsdorfer, W.; Christou, G.; Brechin, E. K. *Chem. Commun.* **2005**, 2083−2085.

(52) Tangoulis, V.; Malamatari, D. A.; Soulti, K.; Stergiou, V.; Raptopoulou, C. P.; Terzis, A.; Kabanos, T. A.; Kessissoglou, D. P. *Inorg. Chem.* **1996**, *35*, 4974−4983.

(53) Birkelbach, F.; Florke, U.; Haupt, H. J.; Butzlaff, C.; Trautwein, A. X.; Wieghardt, K.; Chaudhuri, P. *Inorg. Chem.* **1998**, *37*, 2000−2008.

(54) Miyakasa, H.; Clérac, R.; Wernsdorfer, W.; Lecren, L.; Bonhomme, C.; K., S.; Yamashita, M. *Angew. Chem., Int. Ed.* **2004**, *43*, 2801−2805.

(55) Krzystek, J.; Ozarowski, A.; Telser, J. *Coord. Chem. Rev.* **2006**, *250*, 2308−2324.

speaking, of two halves, one consisting of the Mn(II) moiety and the other of the two Mn(III) ions and their coordination spheres.

Conclusions

In the absence of any other base, the reactivity of the novel heptadentate bis-β-diketone ligand **H_5L** with various transition metal $M(AcO)_2$ salts is very dependent on the nature of the metal. With M = Ni^{II} and Co^{II}, the reaction in pyridine leads to dinuclear complexes $[Ni_2(H_3L)_2(py)_4]$ (**1**) and $[Co_2(H_3L)_2(py)_4]$ (**2**), with the metals within the molecule widely separated from each other (near 8 Å). By contrast, with $Mn(AcO)_2$ the product is a very rare linear $[Mn_4]$ cluster with a zigzag configuration and formula of $[Mn_4(H_2L)_2(AcO)_2(py)_5]$ (**3**), presumably because Mn^{II} is subject to less crystal field constraints to distort its coordination geometry. The same reaction in DMF leads to the analogous cluster $[Mn_4(H_2L)_2(AcO)_2(dmf)_4]$ (**4**), indicating that this arrangement is a robust topology. Complex **3** was found to slowly oxidize and recrystallize in the form of the mixed-valent complex $[Mn_3(HL)_2(py)_6]$ (**5**), which displays a unique asymmetric $Mn^{III}-Mn^{III}-Mn^{II}$ linear sequence. Compound **5** can also be prepared directly by comproportionation from the appropriate amounts of Mn^{VII} and Mn^{II} in the presence of **H_5L**. The paramagnetic ions within **3** and **5** were found, by means of bulk magnetic measurements, to weakly interact as described by small antiferromagnetic coupling constants. The polydentate ligand **H_5L** thus constitutes a suitable scaffold for the preparation of novel linear transition metals in a variety of topologies and nuclearities.

Experimental Section

Syntheses. All reactions were performed in air and using solvents and reagents as received. $NBu^n{}_4MnO_4$ was prepared according to a procedure reported in the literature.[56] ***Warning!*** *Quaternary ammonium permanganates may detonate during drying at elevated temperatures. We therefore recommend using them only in small amounts and that the heating of them be avoided.*

1,3-Bis-(3-oxo-3-(2-hydroxyphenyl)-propionyl)-2-methoxybenzene (H_4L'). Liquid dimethyl 2-methoxyisophthalate (8.40 g, 37.46 mmol) and liquid 2-hydroxyacetophenone (14 mL, 112.38 mmol) were dissolved under argon in anhydrous dimethoxyethane (DME, 200 mL). In a different flask, 60% oil dispersion of NaH (14 g, 360 mmol) was washed twice under argon with hexane and the solvent extracted by means of a filter cannula. To this solid was added anhydrous DME (50 mL) under an inert atmosphere, and the resulting suspension was added carefully with a syringe onto the above mixture, the color turning bright yellow immediately (***CAUTION!!*** *As a result of hydrogen evolution, heavy bubbling occurs upon addition of the NaH suspension; thus, this addition needs to be carried out with extreme caution*). After the addition was complete, the mixture was brought to reflux as it gradually turned orange, and this was maintained overnight. Approximately after 24 h, the mixture was allowed to cool to room temperature and to come into contact with the atmosphere. An abundant yellow precipitate was collected by filtration and washed with DME. This solid was suspended in a biphasic system of EtAcO and water, followed by the addition of 1 M HCl until it acquired an approximate pH = 1. At this point, the solid was completely dissolved and the organic yellow phase was decanted, dried over Na_2SO_4, and rotaevaporated. The resulting yellow-green solid was suspended in acetone (40 mL), and the mixture was boiled for a few minutes. The system was allowed to reach room temperature, and the remaining solid was collected by filtration and washed with a small amount of acetone. The yield was 27% (4.3 g). Anal. Calcd (Found) for **H_4L'**: C, 69.44 (69.06); H, 4.66 (4.16). ESI MS (>0): *m/z* 455 $[M + Na]^+$, 433 $[MH]^+$, 415 $[M - (OH^-)]^+$. FAB MS (>0): *m/z* 433 $[MH]^+$, 401 $[MH- OMe]^+$. ^1H NMR ($CDCl_3$): δ (ppm) = 3.87 (*s*, 3H, CH_3), 6.95 (*t*, 2H, $C_{aro}H$), 7.03 (*d*, 2H, $C_{aro}H$), 7.15 (*s*, 2H, CH), 7.37 (*t*, 1H, $C_{aro}H$), 7.50 (*t*, 2H, $C_{aro}H$), 7.78 (*d*, 2H, $C_{aro}H$), 7.97 (*d*, 2H, $C_{aro}H$), 12.04 (*s*, 2H, C_{aro}-OH), 15.52 (*s*, 2H, $C_{enol}OH$).

1,3-Bis-(3-oxo-3-(2-hydroxyphenyl)-propionyl)-2-methoxybenzene (H_5L). A round-bottomed flask containing **H_4L'** (400 mg, 0.96 mmol) and CH_2Cl_2 (20 mL) was purged with argon and cooled with an ice bath. To this mixture was added very carefully a 1 M solution of BBr_3 in MeOH (1.5 mL, 1.5 mmol) with a syringe. An orange precipitate started to form immediately. The mixture was stirred vigorously for 3 h while the ice bath melted. The mixture was further washed with CH_2Cl_2 and dumped into an ice bath containing an aqueous solution of NaCl. After the whole system was stirred for another 4 h, the two phases formed were separated and the organic part was rotaevaporated to obtain a dark glassy film. This film was dissolved in the minimum amount of CH_2Cl_2, to the solution was added MeOH (20 mL), and the mixture was left to stand at 4 °C. After 2 days, yellow crystals were collected by filtration. The yield was 40%. Anal. Calcd (Found) for **H_5L** ($C_{24}H_{18}O_7$): C, 68.90 (69.06); H, 4.34 (4.16). ESI MS (>0): *m/z* 419 $[MH]^+$, 401 $[M - (OH^-)]^+$. ^1H NMR ($CDCl_3$): δ (ppm) = 4.72 (*s*, 2H, CH_2), 6.92 (*t*, 1H, $C_{aro}H$), 6.98 (*t*, 1H, $C_{aro}H$), 6.99 (*d*, 1H, $C_{aro}H$), 7.04 (*d*, 1H, $C_{aro}H$), 7.10 (*t*, 1H, $C_{aro}H$), 7.46 (*t*, 1H, $C_{aro}H$), 7.54 (*s*, 1H, CH), 7.55 (*t*, 1H, $C_{aro}H$), 7.79 (*d*, 2H, $C_{aro}H$), 7.96 (*d*, 1H, $C_{aro}H$), 8.31 (*d*, 1H, $C_{aro}H$), 11.77 (*s*, 1H, $C_{aro}OH$), 12.03 (*s*, 1H, $C_{aro}OH$), 13.32 (*s*, 1H, $C_{aro}OH$), 15.56 (*s*, 1H, $C_{enol}OH$).

$[Ni_2(H_3L)_2(py)_4]$ (1). Solid $Ni(AcO)_2\cdot 4H_2O$ (32 mg, 0.13 mmol) and **H_5L** (26 mg, 0.06 mmol) were mixed in pyridine (5 mL) and stirred for a few minutes. The green solution was layered with ether, and after a few days, green crystals suitable for X-ray crystallography had settled, which were then collected by filtration, washed with ether, and dried in air. The yield was 40%. Anal. Calcd (Found) for **1**·py ($C_{73}H_{57}N_5O_{14}Ni_2$): C, 65.16 (64.87); H, 4.27 (4.45); N, 5.20 (5.39).

$[Co_2(H_3L)_2(py)_4]$ (2). Solid $Co(AcO)_2\cdot 4H_2O$ (32 mg, 0.13 mmol) and **H_5L** (26 mg, 0.06 mmol) were mixed in pyridine (5 mL) and stirred for a few minutes. The orange solution was layered with ether, and after a few days, orange crystals suitable for X-ray crystallography had grown, which were then collected by filtration, washed with ether, and dried in air. The yield was 34%. Anal. Calcd (Found) for **2** ($C_{68}H_{52}N_4O_{14}Co_2$): C, 64.46 (64.20); H, 4.14 (4.15); N, 4.42 (4.98).

$[Mn_4(H_2L)_2(AcO)_2(py)_5]$ (3). Solid $Mn(AcO)_2\cdot 4H_2O$ (32 mg, 0.13 mmol) and **H_5L** (26 mg, 0.06 mmol) were mixed in pyridine (10 mL) and stirred for a few minutes. The orange solution was layered with ether, and after a few days, orange crystals suitable for X-ray crystallography were deposited, which were then collected by filtration, washed with ether, and dried in air. The yield was 30%. Elemental analysis reveals partial substitution of pyridine by water upon exposure to air. Anal. Calcd (Found) for **1** (−1.5py +

---

(56) Vincent, J. B.; Folting, K.; Huffman, J. C.; Christou, G. *Inorg. Chem.* **1986**, *25*, 996.

$1.5H_2O$); ($C_{69.5}H_{56.5}N_{3.5}O_{19.5}Mn_4$): C, 56.69 (56.86); H, 3.87 (3.68); N, 3.33 (3.09).

[$Mn_4(H_2L)_2(AcO)_2(dmf)_4$] (4). The same procedure as above was carried out in DMF instead of pyridine. Orange crystals of **4** were obtained from the DMF/Et_2O layers after a few days. The yield was 26%. Anal. Calcd (Found) for **4** ($C_{64}H_{64}N_4O_{22}Mn_4$): C, 52.62 (52.23); H, 4.42 (4.52); N, 3.83 (3.85).

[$Mn_3(HL)_2(py)_6$] (5). Method 1. The py/Et_2O layers leading to complex **3** were left unperturbed for about a month. During this time, the orange crystals of **3** slowly redissolved with concomitant recrystallization of dark brown crystals of **5**. At the end of that period, all orange crystals had disappeared, the only solid present in the system being the brown crystals. These were suitable for X-ray crystallography (synchrotron radiation source). This product was collected by filtration. The yield was 25%. Anal. Calcd (Found) for **5**·py ($C_{83}H_{63}N_7O_{14}Mn_3$): C, 64.43 (64.20); H, 4.09 (4.09); N, 6.34 (6.44).

Method 2. Solid Bu_4NMnO_4 (9 mg, 0.03 mmol) and $Mn(AcO)_2\cdot 4H_2O$ (40 mg, 0.16 mmol) were mixed and dissolved in pyridine (7 mL) to produce a dark brown solution. To this mixture was added a solution of **H_5L** (52 mg, 0.13 mmol) in pyridine (13 mL). The resulting brown solution was stirred for about 30 min and layered with Et_2O. After a week, crystals of **5** had deposited, which were collected by filtration. The yield was 24%.

Physical Measurements. Field-cooled measurements of the magnetization of smoothly powdered microcrystalline samples of **3** and **5** were performed in the range of 2−300 K with a Quantum Design MPMS-5XL SQUID magnetometer with an applied field of 5 kG. Corrections for diamagnetic contributions of the sample holder to the measured magnetization and of the sample to the magnetic susceptibility were performed experimentally and by using Pascal's constants, respectively. Measurements under an ac magnetic field in the 2−40 K range at 1339 and 107 Hz were also performed. IR spectra were recorded as KBr pellet samples on a Nicolet 5700 FT-IR spectrometer. Elemental analyses were performed in-house on a Perkin-Elmer Series II CHNS/O Analyzer 2400, at the Servei de Microanàlisi of CSIC, Barcelona, Spain.

X-ray Crystallography. Pertinent data for the structure determinations are given in Table 1. Data of **H_5L**, **1**, and **3** were collected on a Nonius KappaCCD diffractometer on rotating anode (graphite-monochromated Mo Kα radiation, $\lambda = 0.71073$ Å). Data were collected at 150 K. The structures were solved with direct methods using SHELXS86[57] (compounds **H_5L** and **1**) or SHELXS97[58] for structure **3**. Refinement on F^2 was performed with SHELXL-97.[59] The hydroxyl hydrogen atoms of **1** and **3** and all hydrogen atoms of **H_5L** were located on a difference-Fourier map, and their coordinates were included as parameters in the refinement; all other hydrogen atoms were included on calculated positions riding on their carrier atoms. Structure **3** showed a large area of disordered solvent for which no satisfactory atomic model could be obtained. The contribution of the disordered solvent to the scattered intensity was taken into account with the SQUEEZE procedure, as incorporated in PLATON.[60] Neutral atom scattering factors and anomalous dispersion corrections were taken from the International Tables for Crystallography.[61] Validation, geometrical calculations, and illustrations were performed with PLATON.[60]

For complexes **2**, **4**, and **5**, data were collected at 150 K (**2** and **5**) or 180 K (**4**) using a Bruker APEX II CCD diffractometer on station 9.8 (**4** and **5**) or 16.2 smx (**2**) of the Synchrotron Radiation Source at CCLRC Daresbury Laboratory, at 0.8464 (**2**), 0.6711 (**4**), and 0.6894 (**5**) Å, from a Silicon 111 monochromator. The structure was solved by direct methods and refined using the SHELXTL[62] suite of programs. All non-H atoms of complex **4** (except those in a solvent molecule) are anisotropic. Hydrogens were placed geometrically where possible; for the CH_3 groups, the hydrogens were found in the rotational difference map. For the OH, the hydrogen was placed to form the best hydrogen bonds and then refined using a riding model. The H atoms on the water molecule can neither be geometrically placed nor found in the difference map and were therefore omitted. For complex **5**, all non-hydrogen atoms were modeled isotropically except the partial water molecule and the very disordered pyridine site. The hydrogens were placed geometrically where possible with the exception of the two hydroxyl groups where the hydrogens were found in the difference map, and those of the partial water which could not be placed or found in the difference map were therefore omitted from the refinement. All hydrogens were then constrained and refined using a riding model. Both geometrical and displacement parameter restrains were used in the modeling of the disordered pyridine. A peak of 2.9 e^- remains in the different map at 1.2 Å from the one on the Mn atoms, which is in an unreasonable position for sensible modeling. Inspection of the final refinement does indicate that there is probably a small degree of twinning present; e.g., K values in analysis of variance for reflection are higher than 1 for F_c/F_{max} and F^2_{obs} is larger than F^2_{calc} for the weak data, where no suitable twin law could be found. This twinning probably accounts for the 2.9 e^- peak left in the difference map.

Electron Paramagnetic Resonance. The X-band EPR spectrometer was a commercial Bruker ElexSys E680X product, equipped with an Oxford Instruments helium-flow cryostat and a dielectric FlexLine resonator. The HFEPR instrument was a home-built device, described elsewhere.[63] The latter instrument operates in transmission mode and employs no resonator.

Acknowledgment. This work was supported by Spanish Ministerio de Ciencia y Tecnología through Grant No. BQU 2003/00539 and a "Ramón y Cajal" contract (G.A.) by the Council for the Chemical Sciences (A.L.S.) of The Netherlands Organization for Scientific Research (CW-NWO). We acknowledge the provision of time at the CCLRC Daresbury Laboratory via the support by the European Union. EPR studies were supported by the National High Magnetic Field Laboratory, which is funded by the National Science Foundation through Cooperative Agreement DMR 0084173, the State of Florida, and the Department of Energy.

Supporting Information Available: CIF file; PDF file containing additional information including Figures S1−S3. This material is available free of charge via the Internet at http://pubs.acs.org.

IC062075V

---

(57) Sheldrick, G. M. *SHELXS86;* University of Göttingen: Göttingen Germany, 1986.

(58) Sheldrick, G. M. *SHELXS97*; University of Göttingen: Göttingen, Germany, 1997.

(59) Sheldrick, G. M. *SHELXL-97*; University of Göttingen: Göttingen, Germany, 1997.

(60) Spek, A. L. *J. Appl. Cryst.* **2003**, *36*, 7−13.

(61) *International Tables for Crystallography*; Kluwer Academic Publishers: Dordrecht, The Netherlands, 1992; Vol C.

(62) Bruker AXS: Madison, WI, 2005.

(63) Hassan, A. K.; Pardi, L. A.; Krzystek, J.; Sienkiewicz, A.; Goy, P.; Rohrer, M.; Brunel, L. C. *J. Magn. Reson.* **2000**, *142*, 300−312.